Kinetically Controlled Assembly of Terpheny-4,4"-dithiol Self-Assembled Monolayers (SAMs) for Highly Conductive Anisotropically Conductive Adhesives (ACA)

Joshua C. Agar, Jessica Durden, Rongwei Zhang, Daniela Staiculescu and C. P. Wong
School of Materials Science and Engineering, Georgia Institute of Technology
771 Ferst Drive, Atlanta, GA, 30332, USA
Phone: 404-894-8391, Fax: 404-894-9140, E-mail: cp.wong@mse.gatech.edu

Abstract

Anisotropically conductive adhesives (ACA) are a promising alternative to solder interconnects for high performance electronic devices due to their increased I/O capabilities and reduced form factor. Previous studies have shown that modification of Au coated Ni/Cu bumps with conjugated self-assembly monolayers (SAMs) increases conductivity, current carrying capacity and reliability of ACA interconnects[1-3]. In this study, we kinetically control the assembly of p-Terphenyl-4,4"-dithiol (TPD) monolayers on Au bumps. Using a custom designed test vehicle we show how TPD SAMs can either increase or decrease the single bump resistance depending on the kinetics of the monolayer formation and its resulting structure. Future studies focusing on controlling monolayer assembly will determine the efficacy of conjugated SAMs at enhancing the conductivity and current carrying capacity of ACA interconnects.

Introduction

Ultrafast electronic devices are constantly striving for improved performance, reduced form factor and decreased cost. Increasing interconnectivity between electronic components by reducing pitch is the ideal method to increase processing capabilities of electronic devices. One of the most simple and economical technologies to produce fine pitch (<40 μm) interconnects is anisotropically conductive adhesives/films (ACA/ACF). ACF is prepared by suspending conductive particles within a polymer matrix. Interconnection is established when particles are trapped between bumps on the substrate and integrated circuit (IC) during a flip chip thermo-compression bonding process. Because ACFs have a low density of conductive fillers and the diameter of the bump is much larger than the particles, the cured film is conductive only in the direction perpendicular to the substrate. The anisotropic nature of the conductivity limits the pitch of the interconnects to the fabrication and alignment capabilities. A schematic drawing of the cross-section of an assembled ACF interconnect is shown in Figure 1.

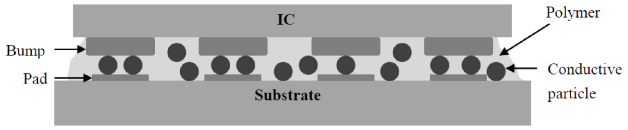

Figure 1. Schematic drawing of ACF interconnects.

ACF interconnection has numerous advantages over traditional solder interconnection. ACF interconnects are lead-free, require low processing temperatures and are more environmentally friendly than solder interconnects [4]. Currently, ACF materials are commercially used in a wide range of low powered commercial devices such as smart cards and liquid crystal displays [4]. However, ACF technology has not been implemented in high-powered electronic devices due to its lower conductivity and current carrying capacity when compared to conventional solder interconnects. For ACF to be a viable replacement for conventional interconnect technology, improved conductivity and current carrying capacity is mandatory.

Unlike direct metallic contact, the conduction mechanism in ACF joints is highly complex. The complexity results from the complex mechanical and electrical interactions between the polymer matrix, filler and bumps. Extensive analysis of the mechanics of ACF interconnection and assembly has been published[5-8]. However, researchers have been unable to develop a model that accurately predicts the conduction mechanism in ACF interconnects.

Many published theoretical models have assumed connection is formed through a combination of contact resistance R_c and tunneling resistance R_t [9]. Constriction resistance is defined as the resistance resulting from the current flow being confined to the small area where metallic contact exists. The tunneling resistance is defined as the resistance for an electron to tunnel through a thin layer of polymer separating the conductive particles and the metallic electrodes. Many journal articles published on the conduction mechanism in ACF interconnects have made the incorrect assumption that the tunneling resistance and constriction resistance add in series [9]. Instead a more correct model would assume that conduction via a constricted metallic contact and tunneling occurs in parallel. The proposed model for the electrical conduction mechanism in ACF interconnects is shown mathematically in Eq. 1 and graphically in Figure 2; where R_c is the contact resistance, R_t is the tunneling resistance and R_p is the resistance of the particle.

$$R = \sum \left[\frac{1}{R_c} + \frac{1}{R_t}\right]^{-1} + R_p \quad (1)$$

Descriptions of the contact resistance can be defined as shown in Eq. 2, where ρ is the resistivity of the contacting bodies and a is the radius of the contact area [9].

$$R_c = \frac{\rho}{4a}\Omega \quad (2)$$

The mathematical interpretation of the tunneling resistance is much more complex due to the variety of tunneling/electron transport mechanisms which occur competitively. One simplistic model that has been used to describe tunneling resistance in ACF interconnects is the Simmons model [10]. This model describes the conductivity due to tunneling as a function of the film thickness in Å (s), work function (Φ) and dielectric constant of the film ε_r, as shown in Eqs. 3-5.

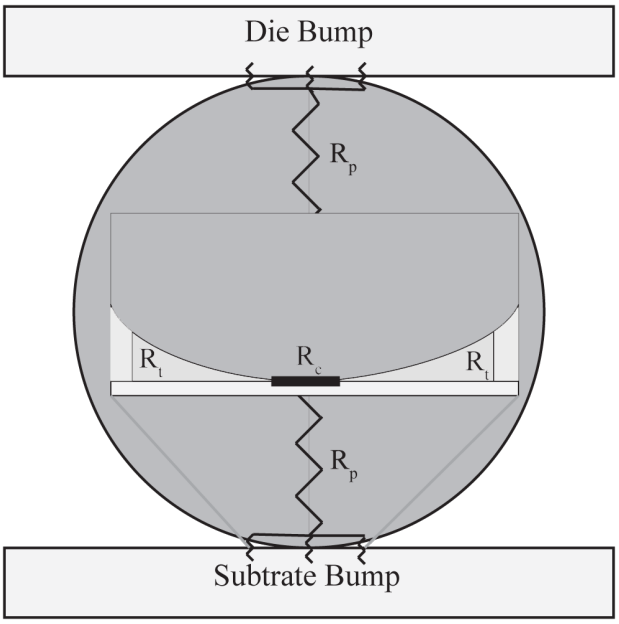

Figure 2. Schematic drawing of hypothesized conduction mechanism in ACF interconnects.

$$\sigma = \sigma(s, \Phi, \varepsilon_r) = \frac{10^{-22}}{2} \frac{A^2}{1 + AB} e^{AB}\ \Omega\ \text{cm}^2 \quad (3)$$

$$A = 7.32x10^5 \left(s - \frac{7.2}{\Phi}\right) \quad (4)$$

$$B = 1.265x10^{-6} \sqrt{\Phi - \frac{10}{s\varepsilon_r}} \quad (5)$$

Recently, it has been shown that surface modification of noble metal bumps and conductive fillers with self-assembled monolayers (SAMs) increases the conductivity and current carrying capacity of ACF interconnects [1-3]. SAMs are ordered 2D structures of oligomers that form spontaneously on noble metal surfaces in solution or gas phase. These oligomers contain three functional segments which aid in their self-assembly. These functional groups include: a chemically reactive head group, which forms a strong physiochemical bond with noble metal surfaces; a backbone, whose van der Waals interactions cause the molecules to align on the surface and a terminal group which has chemical functionality. Many chemically functional moieties can be used to form SAMs; however, our analysis will be limited to thiol (-SH) terminated SAMs on Au surfaces.

The formation of SAMs is a dynamic kinetically controlled process. The rate of monolayer formation is highly dependent on the enthalpy of adsorption, van der Waals interaction, concentration, solvent, temperature, etc. Despite these complexities, the SAM adsorption process can be described by the simplistic first-order Langmuir adsorption isotherm as shown in equations 6-7, where θ is the fraction of occupied sites, t is the time, t_c is the time when growth starts and k is the rate constant, which is dependent on both the adsorption attempt frequency and frequency of attempts that result in adsorption [11].

$$\frac{d\theta}{dt} = -k(1 - \theta) \quad (6)$$

$$\theta = 1 - \exp -k(t - t_c) \quad (7)$$

Conjugated SAM modification of bump surfaces enhances conduction in ACF joints via two different mechanisms. First, the adsorption of well-ordered SAMs on metallic electrodes has been reported to alter the work function of the metallic surfaces [12].

Work function modulation is caused by the formation of aligned, oriented, interface dipoles on the surface of the metallic bump/particle surface [12]. Through work function modulation, the electron (hole) injection barriers can be modulated, facilitating charge transport. To maximize the effect of work function modulation the SAM molecules must be oriented such that the interface dipole is perpendicular to the bump surface.

A second plausible mechanism is that conjugated thiol SAMs serve as sites for charge transport. Because these conjugated molecules can accommodate additional electrons in localized states, they can serve as sites for electrons to tunnel and move through. Moreover, because these localized electron states are located closer to the metallic surface than the metallic particles, these molecules facilitate electron transport through a series of short tunneling/hopping events on the SAM molecule. A sequence of short tunneling/hopping events has a higher probability of occurrence than a single tunneling event over the entire insulating barrier due to the exponential decaying tunneling probability with increasing barrier width.

Conduction through conjugated SAMs via tunneling/hopping mechanisms is highly dependent on the molecular coupling of π orbitals. Conduction occurs more quickly when π orbitals are coupled because coupling reduces the energy difference between states and reduces the reorganization energy associated with electron localization.

Because both of these mechanisms of conductivity enhancement are highly dependent on the monolayer crystallography, orientation, tilt angle and density, achieving ideal electrical properties requires precise control of the self-assembly process.

We show a rigorously controlled experiment to determine the efficacy of kinetically controlled SAM of p-Terphenyl-4,4"-dithiol (Figure 3) to enhance the electrical properties of ACF interconnects. Furthermore, via surface analysis we elucidate some of the difficulties associated with applying molecular scale assembly on electrical components fabricated with conventional microelectronic fabrication techniques.

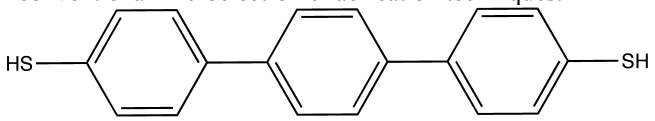

Figure 3. Molecular structure of p-Terphenyl-4,4"dithiol.

Test Structure Design

The regularity and uniformity of the flip chip test structure is paramount in producing statistically significant results. Our design consisted of two chips with matching bumps. For the remainder of this paper we will refer to the bottom chip containing the pads as the substrate and the matching top chip containing the daisy chained bumps as the die. Both the die

and the substrate contained four test regions each consisting of three bumps. The bumps on the die are 90 µm in diameter with a 110-micron pitch (edge to edge). On the substrate the bumps are 120 µm in diameter with an 80-micron pitch (edge to edge). Upon flip chip assembly the three bumps were interconnected to the substrate such that a four-point measurement could be completed to determine the resistance of the bumps located on the corners. The four-point testing method utilized eliminates any resistance resulting from the metallic traces because the voltage drop is measured from the top of the bump to the point where the two metallic traces split. The design of the test vehicle as well as the four-point testing setup can be seen in Figure 4.

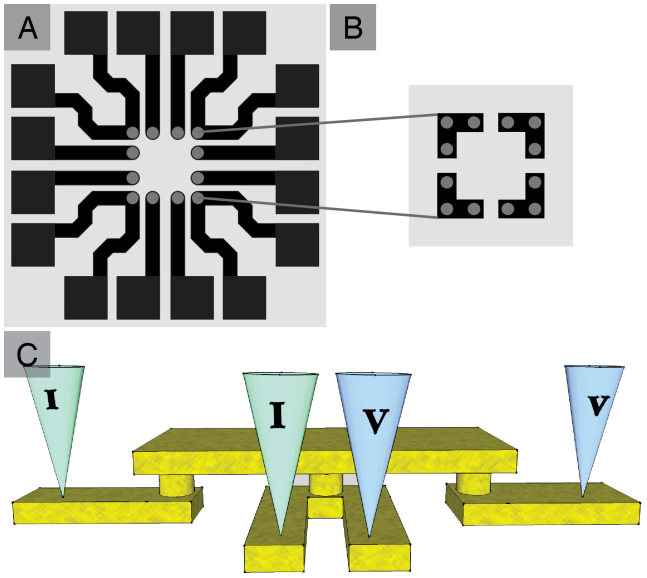

Figure 4. Drawing of A) Test vehicle substrate. B) Test vehicle die. C) Electrical measurement setup.

Moreover, to simplify the assembly process, the bumps were arranged in a square centrally located on the surface of the silicon substrate and die. Since the flip chip bonder utilized a rotating arm to apply the load, the bumps were located near the center of the chips to ensure planarity.

The test structures were fabricated by TLMI Corporation. The metallic structures were initially defined in copper and then coated with an adhesion layer of nickel. The surfaces were finished by coating the structures with a thin layer of gold. The bumps were formed using TLMI proprietary technology to form bumps with a flat surface. The use of flat bumps was essential to minimize any inconsistencies caused by variable contact area and uneven load distribution that can occur when using rounded bumps. Only conventional fabrication processes were used and no special care was made to minimize bump surface roughness. Images of the test structures are shown in figure 5A-B. Figure 5C shows a line plot of a 3D confocal micrograph showing the bump height and the surface topography of the bumps.

Experimental Methods

ACF films were prepared by taking our proprietary formulation consisting of an epoxy matrix, silane coupling agent, Au coated polymer particles swelled with methyl ethyl ketone and toluene. The ACF formulation was screen printed onto a polyethylene terephthalate film, between two pieces of 1 mil thick Kapton tape. Following film preparation residual solvent was allowed to evaporate prior to assembly and bonding.

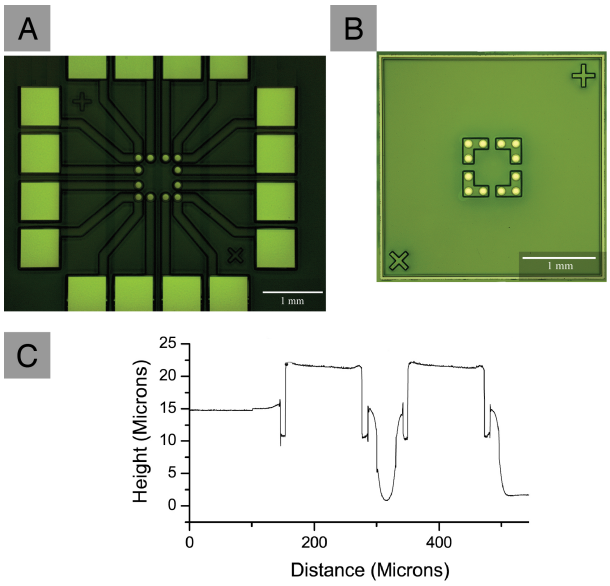

Figure 5. A) Image of test vehicle substrate B) Image of test vehicle die C) Line scan of bump topography acquired with 3D confocal microscope.

Solutions of p-Teraphenol-4-4”-dithiol (TPD) were prepared by creating a 2 mM solution of TDP in toluene and sonicating for 30 minutes until the SAM molecules formed a homogeneous solution. Solutions with concentrations between 1 - $1x10^{-3}$ mM were prepared via a serial dilution in toluene. Surface treatment of test vehicles was accomplished by immersing each test vehicle, face up, in a small glass vial containing 3 ml of p-Teraphenyl-4,4”-dithiol dissolved in Toluene. Surface treatment was conducted for 24 hours in a nitrogen atmosphere. Immediately prior to assembly the samples were removed from solution, washed with toluene and dried. Prior to assembly all test vehicles were inspected to make sure the bump surfaces were pristine. Presence of the adsorbed monolayer was confirmed using a Thermo k-alpha XPS (Thermo Scientific). Surface analysis of the treated and untreated bump surfaces was conducted using a Dimension Edge AFM (Bruker) in contact mode with a SiN tip and in conductive mode using a PtIr coated Si tip.

Flip chip assembly was conducted using a Fineplacer (Finetech) with a fixed gimbal. Once the die and the substrate were aligned a small pieces of ACF film was placed face down on the bumps such that the ACF covered all of the bumps. The sample was heated at 80°C for 5 seconds to adhere the ACF to the substrate. Following pre-cure the PET film was carefully removed from the ACF film. Assembly was completed by applying a force of 20 N via a load arm and curing at 160°C for 5 minutes.

Following assembly, electrical testing was conducted via the four-point probe method to obtain a single bump

resistance. I-V curves for each sample were obtained by applying a variable current from 0 A to 1.5 A and measuring the voltage drop across a single bump using a Keithley 2612B (Keithley Instruments Inc., Cleveland, Ohio). For each sample 1000 data points were collected at 50-ms intervals. I-V curves were plotted and the resistance values were extracted from the linear fit of these plots.

Constant current measurements were conducted using the four-point probe method. A constant current of 5 A was applied using a HP 6553A power supply (HP Hewlett Packard, Palo Alto, CA) and the voltage was measured using a Keithley 2000 multimeter (Keithley Instruments Inc., Cleveland, Ohio). Measurements were taken over a 24-hour period at 90-second intervals.

Maximum current carrying capacity was measured using a HP 6553A power supply (HP Hewlett Packard, Palo Alto, CA) and the voltage was measured using a Keithley 2000 multimeter (Keithley Instruments Inc., Cleveland, Ohio). Current was applied at 1 A intervals for a duration of 30-seconds until interconnect failure.

Results

Control of the surface roughness of the bumps is paramount in forming well-ordered SAMs. SAMs with high crystallographic orientation are obtained when forming SAMs on single crystalline surfaces. The increased order obtained when forming SAMs on single crystalline surfaces results because the SAMs can form a commensurate layer with the underlying surface.

We characterized the bump surfaces of our commercial test vehicle in contact mode using a SiN Tip (Figure 6). Analysis of the surface determined our bumps have an RMS surface roughness of ~28 nm. This degree of surface roughness on a bump is typically not a concern, but in our case it will dramatically affect the assembly, structure and electrical properties of the SAM.

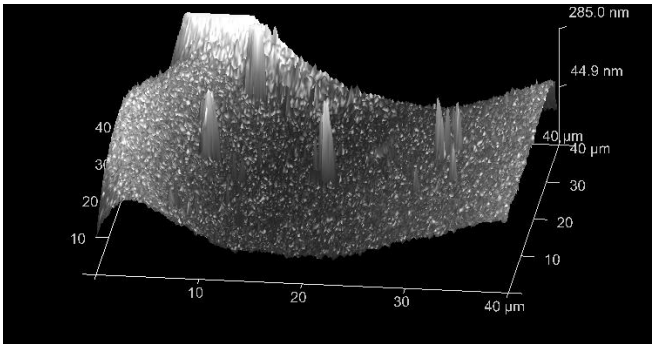

Figure 6. AFM image of surface topography of Au coated bumps. The imaged was acquired using a SiN tip in contact mode.

The degree of surface roughness present on our bump surfaces is too expensive to be avoided for engineering applications. However, this degree of surface roughness interferes with SAM assembly, characterization and the resulting electrical properties of the SAM modified interconnect. The presence of this nanoscale surface roughness complicates AFM characterization of the SAM on Au. Similarly, conductive AFM and scanning capacitance microscopy were cofounded by the large surface roughness. Results from these experiments were difficult to interpret with certainty.

X-ray Photoemission Spectroscopy (XPS) characterization of the sulfur binding energy was difficult to obtain on samples treated with low concentrations (<0.01 mM) of TPD. Typically, obtaining a strong signal of the S-Au bond in SAM is difficult. Characterization of samples treated at higher concentrations showed clear evidence of TPD adsorbed on the Au surface. A high-resolution scan of the S2p region shows a doublet peak a 165.28 eV and 166.08 eV (Figure 7). However, the binding energy of these peaks is too high to be associated with a Au-S bond, with a typical energy of 160.2-161.8 [13]. The peak found is likely the result of free sulfur in TPD adsorbed in multilayers on the surface of the Au bumps. Full elemental analysis of the treated bump surfaces is shown in table I. The low atomic percentage of metals (Au/Cu/Ni) found on the surface indicates that the TPD forms a thick multilayer rather than a monolayer.

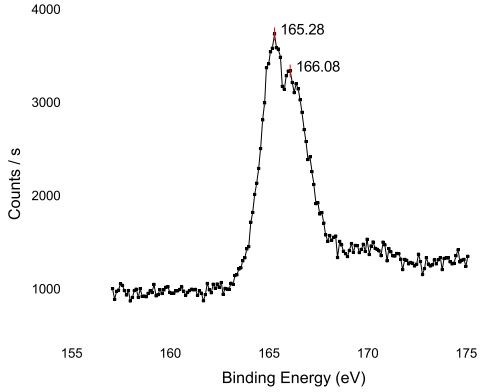

Figure 7. high resolution XPS scan of S2p peak on the bump surface of test vehicle treated with 1 mM TPD for 24 hours. Table shows atomic percentages found by XPS survey scan.

Table I. Survey spectrum of TPD treated bump surface.

Element	C1s	S2p	Cu2p	O1s	Au4f7
Atomic %	87.03	9.1	0.59	2.95	0.33

Following device and electrical assembly as described above single bump resistance for each test region was extracted. A plot of the single bump resistance as a function of the TPD concentration during treatment is shown in Figure 8. In this figure, the rectangle represents the mean, the long central line indicates the median, the longer lines toward the extremities represents the interquartile range and the shorter lines indicate the range. Furthermore, in this figure the black regions indicate the values of the sample and the gray data is a superposition of the control data to aid in visual comparison.

From this graph there are many interesting trends. The typical single bump resistance was less than 1 mΩ, which is comparable or better than previous published values for single bump resistance. However, comparison of single bump resistance is difficult because bump dimensions, design and

fabrication processes are not standardized nor normalized. Comparing the single bump resistance of the untreated control to the test vehicle treated in a 1mM solution of TPD, there is no significant change in single bump resistance.

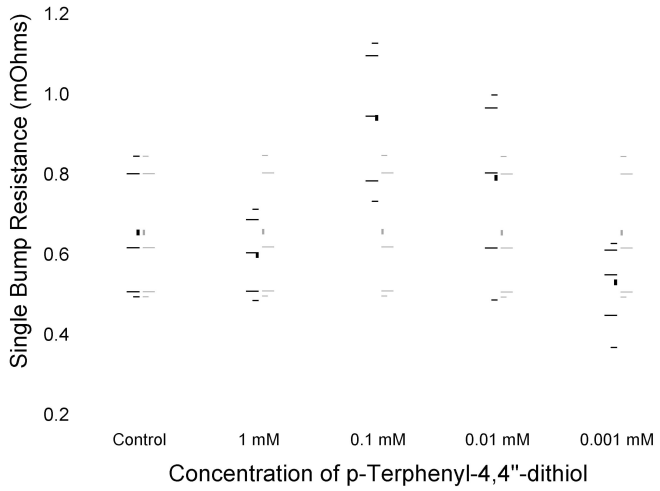

Figure 8. Modified box plot graph showing the change in single bump resistance as a function of TPD concentration during monolayer assembly.

However, upon decreasing the concentration of TPD during assembly the single bump resistance increases significantly. This trend is likely the results of a difference in surface morphology of the SAM. The SAM formed when treating the test vehicles in a 1 mM solution of TPD likely has an ordered monolayer covered by a physically adsorbed multilayer. The higher concentration of TPD in solution causes the adsorption attempt frequency to increase. This increased adsorption attempt frequency results in a more densely packed monolayer. However, the high concentration of TPD in solution also results in multilayer formation. Multilayer formation is common in conjugated SAMs because of the high enthalpy of adsorption associated with π-π stacking [14]. However, these random multilayer structures are insulating, thus they increase the contact and electron hopping/tunneling resistance. Ideally, it would be preferred to have a highly ordered, densely packed monolayer to facilitate charge transport because high density monolayers decrease the hopping distance associated with inter-chain electron transport and reduce molecular reorganization and relaxation associated with electron hopping.

Reducing the concentration of TPD during monolayer assembly effectively reduces the multilayer but also results in a lower density monolayer. Thus, is it likely that the increase in single bump resistance when decreasing TPD concentration is the result of reduced monolayer formation kinetics, leading to lower density monolayers underneath multilayer assemblies.

Finally, at the lowest concentration tested, 0.001 mM we noticed a significant improvement in single bump resistance compared to the control sample. At low TPD concentrations multilayer formation is limited. This evidence is also supported by our inability to find a strong S2p peak in XPS on samples treated with 0.001 mM solution of TPD. The reduced multilayer formation, when treating the bump surfaces in highly diluted solutions of TPD, allows the monolayer to facilitate electron transport, increasing the conductivity of the interconnect. Through external control of the adsorption kinetics such as temperature and electrical potential modulation, it is possible to maximize monolayer density, orientation and crystallinity while reducing multilayer formation [15].

There is a lot of interest to adapt ACF technology for high-powered electronic devices like microprocessors because of their reduced pitch compared to solder. However, ACF materials are still not able to meet the requirements for current carrying capacity necessary for high-powered electronics. We attempted to measure the current carrying capacity of the prepared interconnects but were unsuccessful due to experimental limitations. Constant current measurements on assembled control sample showed stable performance when 5 A of current was applied for >48 hours. Furthermore, the interconnects showed stable performance up to 13 A for 30 seconds, before failing at the probe-pad interface. Because the current carrying capacity of all samples tested failed at the probe-pad interface no conclusions regarding the single bump current carrying capacity could be made.

We show through kinetic control of the self-assembly processes of TPD SAMs that conductivity of ACF interconnects can be modulated. Through careful control of the assembly kinetics we show how it is possible to significantly increase conductivity and current carrying capacity of ACF interconnects. Future studies focusing on active methods to control assembly of conjugated SAMs on the surface of Au bumps hold the potential to dramatically enhance conductivity and current carrying capacity of ACF interconnects. These improvements in conductivity and current carrying capacity could enable ACF interconnection to be utilized in high-powered electronic devices like microprocessors.

Conclusions

A new test vehicle was designed to accurately characterize single bump resistance of TPD modified ACF interconnects. We show that due to the large surface roughness on commercially prepared substrates, surface characterization of TDP SAMs is difficult. Experimental measurement of single bump resistance indicates that TPD SAMs can decrease or enhance single bump resistance depending on the structure of the monolayer. Future studies aimed at forming well-ordered, high-density monolayers and reducing multilayer formation of conjugated SAMs on bump surfaces will conclusively assess the efficacy of SAM to enhance single bump resistance and current carrying capacity of ACF interconnects.

References

1. Y. Li, K.-S. Moon, and C. Wong, "Adherence of self-assembled monolayers on gold and their effects for high-performance anisotropic conductive adhesives," *Journal of Electronic Materials,* vol. 34, pp. 266-271, 2005.
2. Z. Rongwei, M. Kyoung-sik, L. Wei, and C. P. Wong, "Electrical properties of ACA joints assisted by conjugated molecular wires," in *Electronic Components*

and Technology Conference, 2009. ECTC 2009. 59th, 2009, pp. 2034-2038.
3. G. Yi Li and C. P. Wong, "Nano-Ag Filled Anisotropic Conductive Adhesives (ACA) with Self-Assembled Monolayer and Sintering Behavior for High," in *Electronic Components and Technology Conference, 2005. Proceedings. 55th*, 2005, pp. 1147-1154.
4. M. J. Yim, Y. Li, K.-s. Moon, K. W. Paik, and C. P. Wong, "Review of Recent Advances in Electrically Conductive Adhesive Materials and Technologies in Electronic Packaging," *Journal of Adhesion Science and Technology,* vol. 22, pp. 1593-1630, 2008.
5. R. L. Jackson and L. Kogut, "Electrical Contact Resistance Theory for Anisotropic Conductive Films Considering Electron Tunneling and Particle Flattening," *Components and Packaging Technologies, IEEE Transactions on,* vol. 30, pp. 59-66, 2007.
6. C. N. Oguibe, S. H. Mannan, D. C. Whalley, and D. J. Williams, "Conduction mechanisms in anisotropic conducting adhesive assembly," *Components, Packaging, and Manufacturing Technology, Part A, IEEE Transactions on,* vol. 21, pp. 235-242, 1998.
7. M. Chin, K. A. Iyer, and S. J. Hu, "Prediction of electrical contact resistance for anisotropic conductive adhesive assemblies," *Components and Packaging Technologies, IEEE Transactions on,* vol. 27, pp. 317-326, 2004.
8. W.-S. Kwon and K.-W. Paik, "Fundamental understanding of ACF conduction establishment with emphasis on the thermal and mechanical analysis," *International Journal of Adhesion and Adhesives,* vol. 24, pp. 135-142, 2004.
9. H. Dong, Y. Li, M. J. Yim, K. S. Moon, and C. P. Wong, "Investigation of electrical contact resistance for nonconductive film functionalized with pi-conjugated self-assembled molecules," *Applied Physics Letters,* vol. 90, pp. 092102-3, 2007.
10. R. Holm, *Electrical Contacts, Theory and Applications*. New York: Springer, 1967.
11. O. Dannenberger, M. Buck, and M. Grunze, "Self-Assembly of n-Alkanethiols: A Kinetic Study by Second Harmonic Generation," *The Journal of Physical Chemistry B,* vol. 103, pp. 2202-2213, 1999.
12. I. H. Campbell, J. D. Kress, R. L. Martin, D. L. Smith, N. N. Barashkov, and J. P. Ferraris, "Controlling charge injection in organic electronic devices using self-assembled monolayers," *Applied Physics Letters,* vol. 71, pp. 3528-3530, 1997.
13. G. Heimel, L. Romaner, J.-L. Bredas, and E. Zojer, "Organic/metal interfaces in self-assembled monolayers of conjugated thiols: A first-principles benchmark study," *Surface Science,* vol. 600, pp. 4548-4562, 2006.
14. D. Käfer, G. Witte, P. Cyganik, A. Terfort, and R. C. Salvarezza., "A Comprehensive Study of Self-Assembled Monolayers of Anthracenethiol on Gold: Solvent Effects, Structure, and Stability," *Journal of the American Chemical Society,* vol. 128, pp. 1723-1732, 2006.
15. C. M. A. Brett, S. Kresak, T. Hianik, and A. M. Oliveira Brett, "Studies on Self-Assembled Alkanethiol Monolayers Formed at Applied Potential on Polycrystalline Gold Electrodes," *Electroanalysis,* vol. 15, pp. 557-565, 2003.